Acta Crystallographica Section A
Foundations of Crystallography
ISSN 0108-7673

Received 7 September 2002
Accepted 2 December 2002

X-ray fluorescence holography: a novel treatment for crystal structure determination

F. N. Chukhovskii[a]* and A. M. Poliakov[b]

[a]Institute of Crystallography, the Russian Academy of Sciences, 117333 Moscow, Leninsky Prospect 59, Russia, and [b]Department of Materials Science, Moscow Institute of Steel and Alloys, 117279 Moscow, Leninsky Prospect 4, Russia. Correspondence e-mail: fchukhov@hotmail.com

It is shown that it is possible to use a linear regression algorithm direct method to solve crystal structures from X-ray fluorescence holography (XFH) data. It is found that, in contrast to conventional X-ray structure determination methods, which do not always work unambiguously, the sustainable method utilizing the XFH data generally provides the unique phase-retrieval structure solution and is able, in many cases, to replace the above for determining both the absolute values (moduli) and phases of structure factors. The XFH (θ, φ) scan with a fluorescing Cu atom from a spherical cluster of a Cu_3Au single crystal, at an energy of 10 keV for the incident unpolarized plane-wave X-radiation, is numerically simulated to test the performance of the method in finding a unique solution for the structure factors involved in the restoration procedure using the linear regression algorithm.

1. Introduction

The basic idea of atom-scale resolving holography was first suggested by Szöke, (1986), who proposed the use of decay processes in excited electron shells of atoms as point sources of monochromatic short-wavelength radiation (*e.g.* photoelectrons, short-wavelength fluorescent X-rays and so on). Radiation illuminating an object that consists of individually scattering atoms provides the interference pattern, which can be interpreted in terms of Gabor's holography scheme (Gabor, 1948). Essentially, the point source and scattering atoms are incorporated into one structure (atom cluster), with the source-to-object distances being of the order of interatomic spacing in solids, and the point source may be located either outside or inside the atom cluster. Theoretically, electron holography was well established in the papers of Barton, (1988, 1991). It is remarkable that, as the hologram is created from a single photoemission point source located on an ordered surface, Barton's transform of the two-dimensional holographic pattern (hologram function) in general yields a three-dimensional picture of the surface atom structure surrounding the emitter. In other words, a hologram recorded in two angular variables can be transformed into three space dimensions of an image, thereby displaying plausible positions of neighbouring atoms (with the twin imaging effect, as for every atom that is at the point $\mathbf{r}_j$ a twin atom at the point $-\mathbf{r}_j$ has to be restored).

Just like electrons, a fluorescent X-ray diffraction pattern is produced as a result of the interference between the point-source wave originally emitted by a single photoexcited atom (reference atom) and the waves singly scattered by neighbouring atoms (object). It may be interpreted as a hologram with the original X-ray fluorescent spherical wave as a reference wave and the scattered waves as the object. The hologram data taken over some spherical surface in the reciprocal $\{\mathbf{k}\}$ space can be normalized as the hologram function $\chi(\mathbf{k}) = [I(\mathbf{k}) - I_0(\mathbf{k})]/I_0(\mathbf{k})$, where $I(\mathbf{k})$ is the X-ray intensity detected for the given wavevector $\mathbf{k}$ and $I_0(\mathbf{k})$ is the corresponding intensity emerging from the fluorescing atom in the absence of an object. Tegze & Faigel (1991) experimentally realized the X-ray fluorescence holography (XFH) direct scheme. As was first shown, XFH may utilize the coherence properties of both the spherical wave (reference wave) emitted by a single fluorescing atom and the spherical waves scattered by neighbouring atoms (object wave), together forming the two-dimensional holographic pattern in the reciprocal $\{\mathbf{k}\}$ space. The modern scheme of a multiple-energy X-ray holography (MEXH) using synchrotron radiation was first proposed by Gog *et al.* (1995). It should be noticed that the modern XFH method is based on reciprocal geometry, where the positions of emitter and detector in the direct scheme of the XFH are inverted. According to Gog, Len *et al.* (1996) and Adams *et al.* (1998), the modern schemes of XFH utilize an incident plane-wave radiation as a reference wave, while fluorescing atoms detect the interference holographic signal. For this, a fluorescence yield depends on both the incidence X-radiation angle and, specifically, its energy, which allows better measurement statistics in the MEXH scheme (see Fig. 1). The X-ray atomic scale holography scheme has been the object of numerous experimental and theoretical studies [see *e.g.* Gog, Menk *et al.* (1996) for references of interest].

In fact, the MEXH original set-up does not avoid the 'parasitic' XFH signal that contributes to the observed X-ray hologram. Adams *et al.* (2000) have suggested recording the holography data during continuous rotation of the sample using many sequential revolutions. As was shown, it allows measurement of the refined XFH signal. On the other hand, the complete solution of the above problem might be the strict synchronism of simultaneous rotations of both the sample and the detector. It should be noticed that in an earlier paper (Novikov *et al.*, 1998) the energy-dispersive detector matched the sample rotation keeping a constant elevation angle of the sample surface whereas the detector position was fixed in the azimuth direction. This led to a superposition of the MEXH pattern and an azimuth scan of the XFH pattern recorded at an exit angle. The observed MEXH patterns were 'an azimuth' mixture of the pure MEXH and XFH signals but it appeared to be possible to subtract the XFH trace from the experimental MEXH data set (Novikov *et al.*, 1998). Recently, in Chukhovskii *et al.* (2002), the theoretical formation of the XFH pattern within the direct geometry is treated in the frame of classical electrodynamics and the experimental Fe $K\alpha$ holograms from an Fe single crystal are used for the atom position mapping inside the unit cell by use of the new modified transform *versus* Barton's transform algorithm.

Despite the large number of attempts to utilize the experimental XFH data for the samples that now exist, very few crystal structures are relevant for good reconstruction imaging. That is why for XFH the Barton transform first suggested for photoelectron holography has not been explored in detail and has often been 'trial and error'. Until now, Barton's transform has not been approved for structure restoration only dealing with the atom position mapping inside the unit cell from the XFH data. Specifically, the XFH differs from the photoelectron holography not only in much higher noise levels but also because of the polarization properties of the X-ray spherical waves generated by scattering atoms, which coherently contribute to the holography signal [the XFH (θ, φ) scan].

Before proceeding further, it is important to clarify some issues about structure determination using conventional X-ray diffraction. It is common in structural crystallography that the experimental moduli of structure factors may only be feasible using the conventional X-ray diffraction techniques.

As is well known, the Fourier transform using the experimental moduli of structure factors with the corresponding phases someway restored determines a crystal structure. In order to solve the central problem of structural crystallography to retrieve the phases of structure factors using their moduli as constraints, diverse mathematical methods are utilized [for instance, a phase structure invariant method, a maximum-entropy method *etc*.; see Giacovazzo, (1998) for details]. Unfortunately, the data set of the structure-factor moduli is non-convex, which is the mathematical reason why the conventional X-ray diffraction methods explore multiple redundant solutions for structure determination if no limits on the phase of any of the structure factors under consideration are imposed (see *e.g.* Landree *et al.*, 1997; Giacovazzo, 1998).

In this paper, we treat the issue of structure determination using the XFH data in the full sense, without placing any limits on the phases of structure factors to be restored. Moreover, we show that the XFH method is all-sufficient since it allows one to determine both the phases and moduli of structure factors in the frame of one restoration procedure, ensuring a unique crystal structure solution. The structure determination issue is treated using simulated XFH data for a small crystalline Cu_3Au cluster with a fluorescing Cu atom. In the scope of the kinematical approach, incident plane-wave X-radiation undergoes first-order scattering at atoms adjacent to a fluorescing Cu atom (see Fig. 2). The interference between the incident plane wave and an ensemble of secondary phase-shifted spherical waves yields a Cu $K\alpha$ fluorescence hologram signal as an XFH (θ, φ) scan.

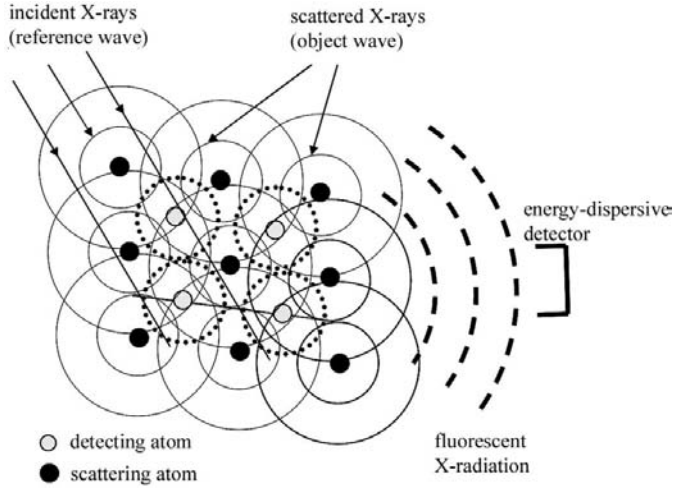

Figure 1
The MEXH scheme proposed by Gog *et al.* (1995), Gog, Len *et al.* (1996) and Gog, Menk *et al.* (1996).

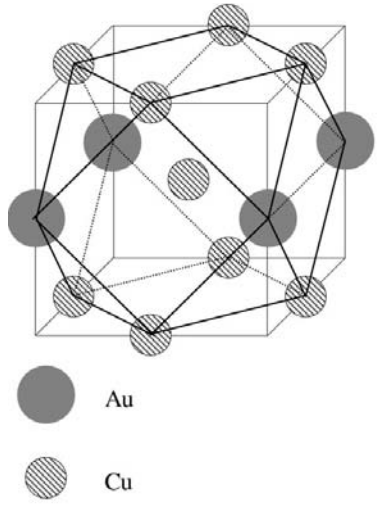

Figure 2
Structure of Cu_3Au with the fluorescing Cu atom at the unit-cell centre.

2. Theoretical background

Let an incident plane wave $\mathbf{E}(\mathbf{r}) = \mathbf{E}_0 \exp(i\mathbf{k}\cdot\mathbf{r})$ be elastically scattered inside a medium and generate an X-ray fluorescence signal from a detecting atom located at the reference point $\mathbf{r} = 0$. Apparently, the wavefield $\mathbf{D}(\mathbf{r})|_{\mathbf{r}=0}$ is a superposition of the incident plane wave (reference wave) and the single-scattered spherical waves (object wave) and is defined within the kinematical approach as:

$$\mathbf{D}(\mathbf{r})|_{\mathbf{r}=0} = \mathbf{E}_0 + (1/4\pi)\int \mathrm{d}^3\mathbf{r}'\,\psi(\mathbf{r}')[-k^2 g(|\mathbf{r}'|)][\mathbf{E}_0 - \mathbf{n}(\mathbf{n}\cdot\mathbf{E}_0)] \times \exp(i\mathbf{k}\cdot\mathbf{r}'), \quad (1)$$

where $g(r) = \exp(ikr)/r$ is the point-like-source function, $\mathbf{k} = k\boldsymbol{\kappa}$ is the wavevector of the incident plane wave, $|\boldsymbol{\kappa}| = 1$, the susceptibility function $\psi(\mathbf{r})$ is defined as $\psi(\mathbf{r}) = -4\pi r_e\rho(\mathbf{r})/k^2$ and is proportional to the electron charge density (ECD) function $\rho(\mathbf{r})$, $\mathbf{r} = r\mathbf{n}$, $|\mathbf{n}| = 1$; r_e is the classical radius of an electron, $r_e = 2.818\times10^{-15}$ m.

In the case of an incident unpolarized plane-wave radiation, the known relationship can be used (Landau & Lifshitz, 1959):

$$\langle E_{0p}E^*_{0q}\rangle = \tfrac{1}{2}|\mathbf{E}_0|^2(\delta_{pq} - \kappa_p\kappa_q) \quad (p, q = 1, 2, 3)$$

(the superscript symbol * means a complex conjugate expression; δ_{pq} is the Kroneker symbol: $\delta_{pq} = 1$ for $p = q$ and $\delta_{pq} = 0$ for $p \neq q$, p, q = 1, 2, 3), and the straightforward evaluations then yield the hologram function as follows [*cf.* the corresponding expression in Adams *et al.* (1998)]:

$$\chi(\mathbf{k}) = r_e\int \mathrm{d}^3\mathbf{r}\,[1 + (\mathbf{n}\cdot\boldsymbol{\kappa})^2]\{\cos[k(\boldsymbol{\kappa}\cdot\mathbf{r} + r)]/r\}\rho(\mathbf{r}). \quad (2)$$

In general, the present expression differs from the corresponding one for the electron hologram function by the polarization-dependent term of $(\mathbf{n}\cdot\boldsymbol{\kappa})^2$ within the integrand of the right-hand side of equation (2). Also, notice that for the traditional XFH scheme the hologram function $\chi(\mathbf{k})$ can be obtained from the above expression by altering the sign of the unit wavevector $\boldsymbol{\kappa}$ in the cosine term of the right-hand side of equation (2).

One step further, we use the Fourier representation of the ECD function $\rho(\mathbf{r})$ as the sum of the reciprocal-space $\rho(\mathbf{h})$ harmonics over the reciprocal diffraction vectors of $\mathbf{h}$ as follows:

$$\rho(\mathbf{r}) = \sum_{\mathbf{h}} \rho(\mathbf{h})\exp(i\mathbf{h}\cdot\mathbf{r}). \quad (3)$$

Noteworthy is the fact that, in many cases, the ECD $\rho(\mathbf{h})$ harmonics may be replaced by the corresponding structure factor $F(\mathbf{h})$ using the well known relationship (V is a crystal unit-cell volume)

$$\rho(\mathbf{h}) = F(\mathbf{h})/V.$$

In the case of a spherical absorbing cluster, and after insertion of (3) into (2), the straightforward evaluations yield

$$\chi(\mathbf{k}) = (2\pi r_e/k^2)\sum_{\mathbf{h}} \rho(\mathbf{h})f(\mathbf{k}, \mathbf{h}),$$
$$f(\mathbf{k}, \mathbf{h}) = f_{\mathrm{spher}}(\mathbf{k}, \mathbf{h}) + f_{\mathrm{polar}}(\mathbf{k}, \mathbf{h}), \quad (4)$$

where each partial $\mathbf{h}$ term of $\rho(\mathbf{h})f(\mathbf{k}, \mathbf{h})$ represents by itself the product of the Fourier ECD $\rho(\mathbf{h})$ harmonics and dimensionless scattering function $f(\mathbf{k}, \mathbf{h})$. The latter in turn is a superposition of two terms, the polarization-independent one [*cf.* the corresponding expression in Adams *et al.* (1998)]:

$$f_{\mathrm{spher}}(\mathbf{k}, \mathbf{h}) = -\frac{k^2}{k^2 - (\mathbf{h} + \mathbf{k})^2} - \frac{k^2}{k^2 - (\mathbf{h} - \mathbf{k})^2} \quad (\mathbf{h} \neq 0); \quad (5)$$

and the polarization-dependent one:

$$\begin{aligned} f_{\mathrm{polar}}(\mathbf{k}, \mathbf{h}) = {} & \{\ln[-i(k + |\mathbf{h} + \mathbf{k}|)] - \ln[-i(k - |\mathbf{h} + \mathbf{k}|)]\} \\ & \times \left(\frac{3k(k^2 + \mathbf{h}\cdot\mathbf{k})^2}{|\mathbf{h} + \mathbf{k}|^5} - \frac{k^3}{|\mathbf{h} + \mathbf{k}|^3}\right) \\ & - \frac{2k^4(k^2 + \mathbf{h}\cdot\mathbf{k})^2}{|\mathbf{h} + \mathbf{k}|^4(k^2 - |\mathbf{h} + \mathbf{k}|^2)} + \frac{2k^2}{|\mathbf{h} + \mathbf{k}|^2} \\ & - \frac{4(k^2 + \mathbf{h}\cdot\mathbf{k})}{|\mathbf{h} + \mathbf{k}|^4} - \{\ln[i(k - |\mathbf{h} - \mathbf{k}|)] \\ & - \ln[i(k + |\mathbf{h} - \mathbf{k}|)]\}\left(\frac{3k(k^2 - \mathbf{h}\cdot\mathbf{k})^2}{|\mathbf{h} - \mathbf{k}|^5} - \frac{k^3}{|\mathbf{h} - \mathbf{k}|^3}\right) \\ & - \frac{2k^4(k^2 - \mathbf{h}\cdot\mathbf{k})^2}{|\mathbf{h} - \mathbf{k}|^4(k^2 - |\mathbf{h} - \mathbf{k}|^2)} + \frac{2k^2}{|\mathbf{h} - \mathbf{k}|^2} \\ & - \frac{4(k^2 - \mathbf{h}\cdot\mathbf{k})}{|\mathbf{h} - \mathbf{k}|^4} \quad (\mathbf{h} \neq 0), \end{aligned} \quad (6)$$

respectively.

Correspondingly, the $\mathbf{h}$-zero partial scattering functions are equal to

$$f_{\mathrm{spher}}(\mathbf{k}, 0) = 0.5, \quad (7)$$

$$f_{\mathrm{polar}}(\mathbf{k}, 0) = 2(0.25 - 2 + \mathbf{C} + \ln 2) \cong -0.9593 \quad (8)$$

($\mathbf{C}$ is Euler's constant, $\mathbf{C}$ = 0.5772156649).

It should be noted that the scattering function $f(\mathbf{k}, \mathbf{h})$ term specified by (4)–(6) as a function of the wavevector $\mathbf{k}$ contain the singularities at the positions of Kossel lines defined by the well known equations $k = |\mathbf{h} \pm \mathbf{k}|$ but not at the 'accidental' points $\mathbf{k} = \pm\mathbf{h}$.

For reference, to calculate the correct partial contribution connected with the reciprocal-lattice vectors of $\pm\mathbf{h}$ to the entire hologram function $\chi(\mathbf{k})$ one needs to summarize both the corresponding ($+\mathbf{h}$) terms and ($-\mathbf{h}$) terms of $\rho(\mathbf{h})f(\mathbf{k}, \mathbf{h})$ and $\rho(-\mathbf{h})f(\mathbf{k}, -\mathbf{h})$ provided that the ECD $\rho(\mathbf{h})$ harmonics identity, $\rho(\mathbf{h}) = \rho(-\mathbf{h})^*$, and the scattering function identity, $f(\mathbf{k}, \mathbf{h}) = f(\mathbf{k}, -\mathbf{h})^*$, take place.

Now a very big difference between the XFH method and conventional X-ray diffraction methods becomes clear in the context of X-ray structure determination. In the case of conventional X-ray diffraction methods, one deals with diffraction patterns where only the moduli sets, $\{|\rho(\mathbf{h})|\}$, are feasible to be measured. Then, for phasing a diffraction pattern, *i.e.* finding the phase set $\{\mathrm{Im}(\ln\rho(\mathbf{h}))\}$, one has to use diverse mathematical procedures, each of which in general yields multiply redundant structure solutions (see *e.g.* Landree *et al.*, 1997; Giacovazzo, 1998). In contrast, the X-ray hologram function $\chi(\mathbf{k})$ depends on a *linear superposition* of the $[\rho(\mathbf{h})f(\mathbf{k}, \mathbf{h}) + \rho(\mathbf{h})^*f(\mathbf{k}, \mathbf{h})^*]$ terms. The latter does mean that X-ray holography may be directly applied to determine structure factors, becoming an *ab initio* technique.

In practice, to put the XFH method into context, one needs to restore the ECD $\rho(\mathbf{h})$ harmonics, $\rho(\mathbf{h}) \equiv \mathrm{Re}(\rho(\mathbf{h})) + i\mathrm{Im}(\rho(\mathbf{h}))$, by using the two-dimensional XFH (θ, φ) scan measured to some high degree of accuracy provided that the absolute value of a wavevector $\mathbf{k}$ is fixed. The 'experimental' data $\chi(\mathbf{k})$ are measured in the form of the XFH (θ, φ) scan where φ is the azimuth angle and θ is the elevation angle of the incident radiation [see Fig. 3 for details; recall that $\mathbf{k} \equiv k\boldsymbol{\kappa}(\theta, \varphi)$, where $|\mathbf{k}t| = k$ and $|\boldsymbol{\kappa}(\theta, \varphi)| = 1$].

Noteworthy is the fact that the above robust equation (2) for the X-ray hologram function does work if the double- and multiple-scattering (extinction) processes of an incident plane wave might be neglected.

3. Linear regression method for restoring structure factors

Let us consider a data set of $\chi_{ij} \equiv \chi(\theta_i, \varphi_j)$ with the array size $I \times J$ (i = 1, 2, 3, . . . , I; j = 1, 2, 3, . . . , J) and introduce the matrices $\hat{\mathbf{A}}(\mathbf{h})$ and $\hat{\mathbf{B}}(\mathbf{h})$, the matrix elements of which are

$$\begin{aligned} A_{ij}(\mathbf{h}) &= 2\mathrm{Re}\, f_{ij}(\mathbf{h}), \\ B_{ij}(\mathbf{h}) &= -2\mathrm{Im}\, f_{ij}(\mathbf{h}). \end{aligned} \tag{9}$$

Correspondingly, (4) can be rewritten in terms of the real and imaginary parts of the ECD $\rho(\mathbf{h})$ harmonics as follows:

$$\chi_{ij} = \sum_n \{A_{ij}(\mathbf{h}_n)\mathrm{Re}(\rho(\mathbf{h}_n)) + B_{ij}(\mathbf{h}_n)\mathrm{Im}(\rho(\mathbf{h}_n))\}, \tag{10}$$

where the sum is taken over the consolidated number $n \equiv (H, K, L)$ of diffraction reflections (the Miller indices H, K, L are integer; for instance: for $L = 1, \ldots, L_{\max}$ and $H = 0, \pm1, \ldots, \pm H_{\max}$ and $K = 0, \pm1, \ldots, \pm K_{\max}$; for $L = 0$ and $H = 0, \pm1, \ldots., \pm H_{\max}$ and $K = 1, \ldots, K_{\max}$; for $L = K = 0$ and $H = 0, 1, \ldots, H_{\max}$, the array size of the reciprocal-lattice vector set N is equal to $4H_{\max}K_{\max}L_{\max} + 2(H_{\max}K_{\max} + H_{\max}L_{\max} + K_{\max}\, L_{\max}) + H_{\max} + K_{\max} + L_{\max})$.

By using the standard least-squares method that in our case reduces to fitting a plane defined by equation (10) to a set of points $\mathrm{Re}\{\rho(\mathbf{h})\}$ and $\mathrm{Im}\{\rho(\mathbf{h})\}$, the so-called *linear regression* procedure (see *e.g.* Barnard & Skillicorn, 1992), one simply inverts (10) into the searching relationship for the real and imaginary parts of the ECD $\rho(\mathbf{h}_m)$ harmonics, namely:

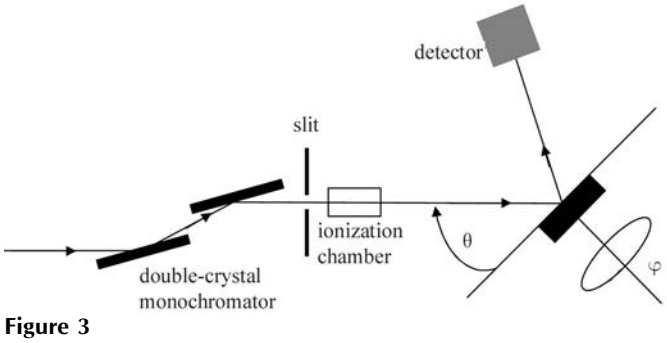

Figure 3
Geometry of the simulated two-dimensional XFH (θ, φ) scan. The azimuth angle φ and the elevation angle θ are measured with respect to the (001) surface of the Cu_3Au sample.

$$\begin{aligned} \mathrm{Re}(\rho(\mathbf{h}_m)) &= \frac{\mathrm{Det}\,\hat{\mathbf{R}}_m}{\mathrm{Det}\,\hat{\mathbf{M}}}, \\ \mathrm{Im}(\rho(\mathbf{h}_m)) &= \frac{\mathrm{Det}\,\hat{\mathbf{I}}_m}{\mathrm{Det}\,\hat{\mathbf{M}}}, \end{aligned} \tag{11}$$

where the matrices $\hat{\mathbf{M}}$, $\hat{\mathbf{R}}_m$ and $\hat{\mathbf{I}}_m$, each with array size $2N \times 2N$, are given by

$$\begin{aligned} \hat{\mathbf{M}} &= \begin{pmatrix} \hat{\mathbf{M}}_{11} & \hat{\mathbf{M}}_{12} \\ \hat{\mathbf{M}}_{21} & \hat{\mathbf{M}}_{22} \end{pmatrix}, \\ \hat{\mathbf{R}}_m &= \begin{pmatrix} \hat{\mathbf{R}}_{m,11} & \hat{\mathbf{M}}_{12} \\ \hat{\mathbf{R}}_{m,21} & \hat{\mathbf{M}}_{22} \end{pmatrix}, \\ \hat{\mathbf{I}}_m &= \begin{pmatrix} \hat{\mathbf{M}}_{11} & \hat{\mathbf{I}}_{m,12} \\ \hat{\mathbf{M}}_{21} & \hat{\mathbf{I}}_{m,22} \end{pmatrix}. \end{aligned} \tag{12}$$

Here the matrices $\hat{\mathbf{M}}_{11}$, $\hat{\mathbf{M}}_{12}$, $\hat{\mathbf{M}}_{21}$ and $\hat{\mathbf{M}}_{22}$, each with array size $N \times N$, are defined as:

$$\begin{aligned} (\hat{\mathbf{M}}_{11})_{nm} &= \sum_{i,j} A_{ij}(\mathbf{h}_n)A_{ij}(\mathbf{h_m})/\langle\varepsilon_{ij}^2\rangle \\ (\hat{\mathbf{M}}_{12})_{nm} &= \sum_{i,j} A_{ij}(\mathbf{h}_n)B_{ij}(\mathbf{h_m})/\langle\varepsilon_{ij}^2\rangle \\ (\hat{\mathbf{M}}_{21})_{nm} &= \sum_{i,j} B_{ij}(\mathbf{h}_n)A_{ij}(\mathbf{h}_m)/\langle\varepsilon_{ij}^2\rangle \\ (\hat{\mathbf{M}}_{22})_{nm} &= \sum_{i,j} B_{ij}(\mathbf{h}_n)B_{ij}(\mathbf{h}_m)/\langle\varepsilon_{ij}^2\rangle \end{aligned} \qquad (n, m = 1, 2, \ldots, N) \tag{13}$$

and the matrices $\hat{\mathbf{R}}_{m,11}$ and $\hat{\mathbf{R}}_{m,21}$, $\hat{\mathbf{I}}_{m,11}$ and $\hat{\mathbf{I}}_{m,21}$, each with the array size $N \times N$, can be obtained from the corresponding matrices $\hat{\mathbf{M}}$ by replacing the mth columns as:

$$\begin{aligned} \hat{\mathbf{R}}_{m,11} = \hat{\mathbf{M}}_{11}| \in (\hat{\mathbf{M}}_{m,11})_{nm} &\Rightarrow \sum_{ij} \chi_{ij}A_{ij}(\mathbf{h}_n)/\langle\varepsilon_{ij}^2\rangle \\ &(n = 1, 2, \ldots, N), \\ \hat{\mathbf{R}}_{m,21} = \hat{\mathbf{M}}_{21}| \in (\hat{\mathbf{M}}_{m,21})_{nm} &\Rightarrow \sum_{ij} \chi_{ij}B_{ij}(\mathbf{h}_n)/\langle\varepsilon_{ij}^2\rangle \\ &(n = 1, 2, \ldots, N), \\ \hat{\mathbf{I}}_{m,12} = \hat{\mathbf{M}}_{12}| \in (\hat{\mathbf{M}}_{m,12})_{nm} &\Rightarrow \sum_{ij} \chi_{ij}A_{ij}(\mathbf{h}_n)/\langle\varepsilon_{ij}^2\rangle \\ &(n = 1, 2, \ldots, N), \\ \hat{\mathbf{I}}_{m,22} = \hat{\mathbf{M}}_{22}| \in (\hat{\mathbf{M}}_{m,22})_{nm} &\Rightarrow \sum_{ij} \chi_{ij}B_{ij}(\mathbf{h}_n)/\langle\varepsilon_{ij}^2\rangle \\ &(n = 1, 2, \ldots, N). \end{aligned} \tag{14}$$

Herein $\langle\varepsilon_{ij}^2\rangle$ is the mean-square error of the XFH χ_{ij} scan measured at the point (i, j).

Thus, the XFH procedure for determining a crystal structure is based upon (11)–(14) with the known (experimentally measured) data set $\{\chi_{ij}\}$ and the scattering matrices $\hat{\mathbf{A}}(\mathbf{h})$ and $\hat{\mathbf{B}}(\mathbf{h})$ given by (4)–(9), which are evaluated within the model of a small crystalline cluster and unpolarized incident plane-wave radiation. Clearly, in the case of centrosymmetric crystals equations (11)–(14) can be reduced by putting $\hat{\mathbf{B}}(\mathbf{h}) = 0$, and only the solutions for structure-factor sets $\{\mathrm{Re}(\rho(\mathbf{h}))\}$ have a sense since $\{\mathrm{Im}(\rho(\mathbf{h}))\} \equiv 0$.

Lastly, 'structure-factor error' equations, albeit not rigorous, that might accommodate counting statistics errors are

required and they are beyond the 'structure-factor' equations (11)–(14). Supposing that the statistical χ_{ij} distribution for each point (i, j) tends to be Gaussian and assuming that r.m.s. errors $\xi_m = \langle[\mathrm{Re}\rho(\mathbf{h}_m)]^2\rangle^{1/2}$, $\eta_m = \langle(\mathrm{Im}\,\rho(\mathbf{h}_m))^2\rangle^{1/2}$ are mutually independent for all the $\mathbf{h}_m$ diffraction reflections, one obtains the following 'structure-factor error' equations [*cf.* equations (11)–(14)]:

$$\begin{aligned}\xi_m &= \mathrm{Det}(\hat{\mathbf{X}}_m)/\mathrm{Det}(\hat{\mathbf{P}}),\\ \eta_m &= \mathrm{Det}(\hat{\mathbf{Y}}_m)/\mathrm{Det}(\hat{\mathbf{P}}).\end{aligned} \tag{15}$$

Here the matrices $\hat{\mathbf{X}}_m$, $\hat{\mathbf{Y}}_m$ and $\hat{\mathbf{P}}$, each with array size $2N \times 2N$, are given by

$$\begin{aligned}\hat{\mathbf{P}} &= \begin{pmatrix}\hat{\mathbf{P}}_{11} & \hat{\mathbf{P}}_{12}\\ \hat{\mathbf{P}}_{21} & \hat{\mathbf{P}}_{22}\end{pmatrix},\\ \hat{\mathbf{X}}_m &= \begin{pmatrix}\hat{\mathbf{X}}_{m,11} & \hat{\mathbf{P}}_{12}\\ \hat{\mathbf{X}}_{m,21} & \hat{\mathbf{P}}_{22}\end{pmatrix},\\ \hat{\mathbf{Y}}_m &= \begin{pmatrix}\hat{\mathbf{P}}_{11} & \hat{\mathbf{Y}}_{m,12}\\ \hat{\mathbf{P}}_{21} & \hat{\mathbf{Y}}_{m,22}\end{pmatrix},\end{aligned} \tag{16}$$

where the matrices $\hat{\mathbf{P}}_{11}$, $\hat{\mathbf{P}}_{12}$, $\hat{\mathbf{P}}_{22}$ and $\hat{\mathbf{P}}_{22}$, each with array size $N \times N$, are defined as:

$$\begin{aligned}(\hat{\mathbf{P}}_{11})_{nm} &= \sum_{i,j} A_{ij}^2(\mathbf{H}_n)A_{ij}^2(\mathbf{H}_m)/\langle\varepsilon_{ij}^2\rangle^2\\ (\hat{\mathbf{P}}_{12})_{nm} &= \sum_{i,j} A_{ij}^2(\mathbf{H}_n)B_{ij}^2(\mathbf{H}_m)/\langle\varepsilon_{ij}^2\rangle^2\\ (\hat{\mathbf{P}}_{21})_{nm} &= \sum_{i,j} B_{ij}^2(\mathbf{H}_n)A_{ij}^2(\mathbf{H}_m)/\langle\varepsilon_{ij}^2\rangle^2\\ (\hat{\mathbf{P}}_{22})_{nm} &= \sum_{i,j} B_{ij}^2(\mathbf{H}_n)B_{ij}^2(\mathbf{H}_m)/\langle\varepsilon_{ij}^2\rangle^2\end{aligned} \qquad (n, m = 1, 2, .., N) \tag{17}$$

and the matrices $\hat{\mathbf{X}}_{m,11}$ and $\hat{\mathbf{X}}_{m,21}$, $\hat{\mathbf{Y}}_{m,12}$ and $\hat{\mathbf{Y}}_{m,22}$, each with array size $N \times N$, can be obtained from the corresponding matrices $\hat{\mathbf{P}}$ by replacing the nth columns as:

$$\begin{aligned}\hat{\mathbf{X}}_{m,11} = \hat{\mathbf{P}}_{11}| \in (\hat{\mathbf{P}}_{m,11})_{nm} &\Rightarrow \sum_{ij} A_{ij}^2(\mathbf{h}_n)/\langle\varepsilon_{ij}^2\rangle\\ &(n = 1, 2, \ldots, N),\\ \hat{\mathbf{X}}_{m,21} = \hat{\mathbf{P}}_{21}| \in (\hat{\mathbf{P}}_{m,21})_{nm} &\Rightarrow \sum_{ij} B_{ij}^2(\mathbf{h}_n)/\langle\varepsilon_{ij}^2\rangle\\ &(n = 1, 2, \ldots, N),\\ \hat{\mathbf{Y}}_{m,12} = \hat{\mathbf{P}}_{12}| \in (\hat{\mathbf{P}}_{m,11})_{nm} &\Rightarrow \sum_{ij} A_{ij}^2(\mathbf{h}_n)/\langle\varepsilon_{ij}^2\rangle\\ &(n = 1, 2, \ldots, N),\\ \hat{\mathbf{Y}}_{m,22} = \hat{\mathbf{P}}_{22}| \in (\hat{\mathbf{P}}_{m,22})_{nm} &\Rightarrow \sum_{ij} B_{ij}^2(\mathbf{h}_n)/\langle\varepsilon_{ij}^2\rangle\\ &(n = 1, 2, \ldots, N).\end{aligned} \tag{18}$$

Noteworthy is the fact that equations (15)–(18) for estimating errors ξ_m and η_m provide means of controlling the progress of the ECD $\rho(\mathbf{h}_m)$ harmonics restoration within the scope of the XFH method based on the measured sets $\{\chi_{ij}\}$, $\langle\varepsilon_{ij}^2\rangle$ and the calculated matrices $\hat{\mathbf{A}}(\mathbf{h}_m)$ and $\hat{\mathbf{B}}(\mathbf{h}_m)$. In fact, equations (15)–(18) might be modified including the error matrix to take into account the correlation effects between errors for different diffraction reflections. At the same time, the above 'structure-factor error' equations seem to be simple enough, giving insight into the accuracy of the plausible ECD $\rho(\mathbf{h}_m)$ harmonics under determination.

Below, the structure determination procedure is attempted by the use of the XFH data set $\{\chi_{ij}\}$ numerically simulated with equations (4)–(8) for the fluorescing Cu atom incorporated into the small spherical crystalline Cu_3Au cluster.

4. Numerical simulation. Results and discussion

The test case we consider is the 'quasi' f.c.c. centrosymmetric Cu_3Au structure commonly used for the XFH experiments (see *e.g.* Novikov *et al.*, 1998; Adams *et al.*, 1998, 2000). The Cu_3Au structure shown in Fig. 2 has a cubic unit cell with the fluorescing Cu atom at the unit-cell centre, the cell parameter a = 0.348 nm. Let the elevation angle of the incident radiation θ be counted from the z axis, $0 \le \theta \le \pi$, the azimuth angle φ be counted around the z axis, $0 \le \varphi < 2\pi$ (see Fig. 3). The true structure factors $F(\mathbf{h})$ for the array size N = 243 specified by the condition $(H^2 + K^2 + L^2)^{1/2} < 5$ were calculated using the analytical X-ray atomic scattering-factor representation

$$f_{\mathrm{Cu(Au)}} = \sum_{u=1,\ldots,5} Q_{\mathrm{Cu(Au)},u} \exp(-P_{\mathrm{Cu(Au)},u}\mathbf{h}^2/16\pi^2) + T_{\mathrm{Cu(Au)}}$$

valid for the full range of $|\mathbf{h}|/2\pi$ from 0.0 to 120.0 nm^{-1} and the corresponding coefficients $T_{\mathrm{Cu(Au)}}$ and $Q_{\mathrm{Cu(Au)},u}$, $P_{\mathrm{Cu(Au)},u}$ for u = 1, 2, ..., 5 are taken from Waasmaier & Kirfel (1995) (for simplicity, the corresponding Debye–Waller factors are put to zero). The entire number N of the true structure factors is equal to 243. Owing to the Cu_3Au structure symmetry (see below), the number of different-valued structure factors is 22 (Fig. 4). The numerically simulated XFH (θ, φ) scans for the 360° azimuth φ, the step $\Delta\varphi = 1$, and the elevation θ from 20 to 90°, the step $\Delta\theta = 1$, at the energy of 10 keV of the incident X-radiation are displayed in Fig. 5. The cases (*a*)–(*c*) of Fig. 5 are related to: (*a*) the partial XFH (θ, φ) scan evaluated using the polarization-independent scattering functions $f_{\mathrm{spher}}(\mathbf{k}, \mathbf{h})$; (*b*) the partial XFH (θ, φ) scan evaluated using the polarization-dependent scattering functions $f_{\mathrm{polar}}(\mathbf{k}, \mathbf{h})$, and (*c*) the

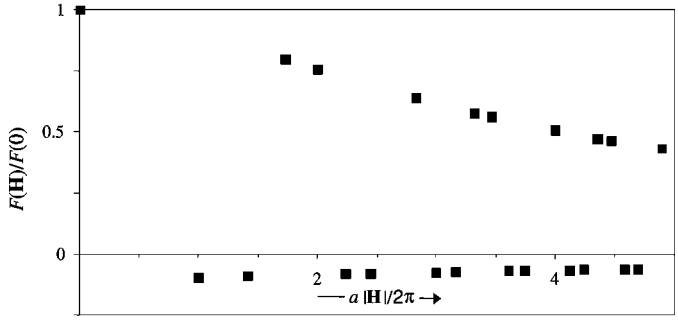

Figure 4
The normalized structure factors, calculated under condition $(H^2 + K^2 + L^2)^{1/2} < 5$ for the Cu_3Au structure are plotted using analytical X-ray atomic scattering-factor representation valid for the full range of $|\mathbf{h}|/2\pi$ from 0.0 to 120.0 nm^{-1} (Waasmaier & Kirfel, 1995). The number of different-value structure factors is 22.

added XFH (θ, φ) scan. It is clearly seen that both the partial XFH (θ, φ) scans comparably contribute to the added XFH (θ, φ) scan. Generally, the numerically simulated XFH pattern is represented by the superposition of Kossel lines, $k = |\mathbf{h} \pm \mathbf{k}|$, that relate to the different reciprocal-lattice vectors $\mathbf{h}$ [see *e.g.* Fig. 6 where the one-dimensional XFH $(\theta = 50^\circ, \varphi)$ scan is depicted]. Because of the fourfold axis symmetry around the [001] direction and mirror plane normal to the [110] direction for the Cu_3Au structure, the XFH (θ, φ) scans possess the azimuth '90° translation' symmetry, and each fourth part of the XFH (θ, φ) scans has the azimuth '45° symmetry' (*cf.* Figs. 5*a–c*).

Then, aiming to test the general restoration procedure, the *m*3*m* point symmetry of the Cu_3Au structure (except for the point symmetry group $\bar{1}$) was ignored and further all the 243 true structure factors contributing to the numerically simulated added XFH (θ, φ) scan in Fig. 5(*c*) were an object of restoration.

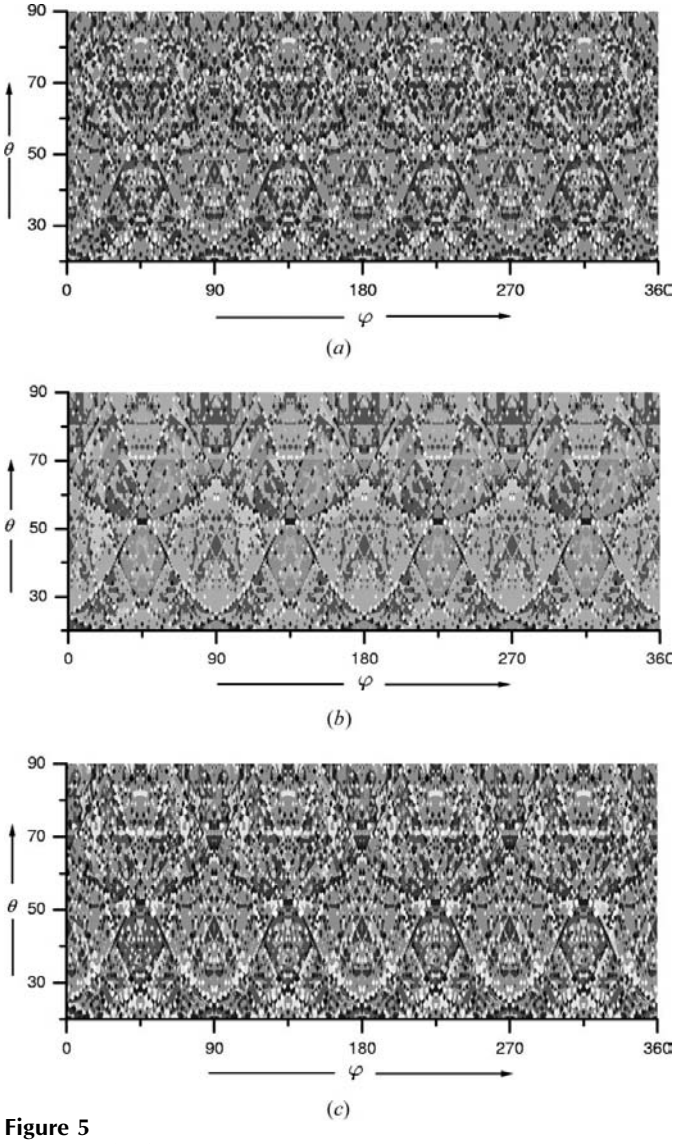

Figure 5
The XFH (θ, φ) scans for the 360° azimuth φ, step $\Delta\varphi = 1$, and the elevation θ from 20 to 90°, step $\Delta\theta = 1$, at an energy of 10 keV for the incident X-radiation, are numerically simulated: (*a*) the polarization-independent XFH (θ, φ) scan; (*b*) the polarization-dependent XFH (θ, φ) scan; (*c*) the added XFH (θ, φ) scan. The fluorescing Cu atom is at the centre of the Cu_3Au unit cell. The total number of diffraction reflections (**h**) contributing to the XFH (θ, φ) scans is 243.

The corresponding scattering functions $f(\mathbf{k}, \mathbf{h})$ were explored to prepare the matrix $\sum_{i,j} A_{ij}(\mathbf{h}_n) A_{ij}(\mathbf{h}_m)$ and the vector column $\sum_{i,j} \chi_{ij} A_{ij}(\mathbf{h}_n)$ for solving the linear matrix equation [see equations (11)–(14)]. For the sake of simplicity, while solving the linear matrix equation for structure factors, all the mean-square errors $\langle \varepsilon_{ij}^2 \rangle$ were assumed to be the same and constant. Accordingly, using the linear regression algorithm code (Barnard & Skillicorn, 1992), all the 243 structure factors of interest were restored. The relative errors of the non-zero structure factors restored were in general equal to 10^{-5}–10^{-6}. Owing to the *m*3*m* point symmetry of the Cu_3Au structure, 25 structure factors are crystallographically different and only 22 are different valued amid the 243 structure factors under restoration. The relative errors and values of the restored 25 structure factors (22 different-valued ones) in comparison with the true ones are listed in Table 1.

5. Concluding remarks

In this paper, the goal of our study is to unveil a good XFH method for purposes of structural X-ray crystallography. The key point of the XFH is the fact that it provides a robust unambiguous procedure to solve a crystal structure. The test above carried out in a linear regression algorithm fashion in the case of a numerically simulated XFH (θ, φ) scan for the small spherical crystalline Cu_3Au cluster leads to an optimistic conclusion. In fact, the non-hybrid XFH method is really unambiguous to restore both the moduli and phases of the crystal structure factors and becomes an *ab initio* technique. It is essential that as the conventional X-ray diffraction techniques utilize rather complicated and sophisticated mathematical models, the XFH method does work well for the structure-factor determination using the linear regression algorithm code.

A few final comments are appropriate here about the implementation of the present mathematical algorithm to the

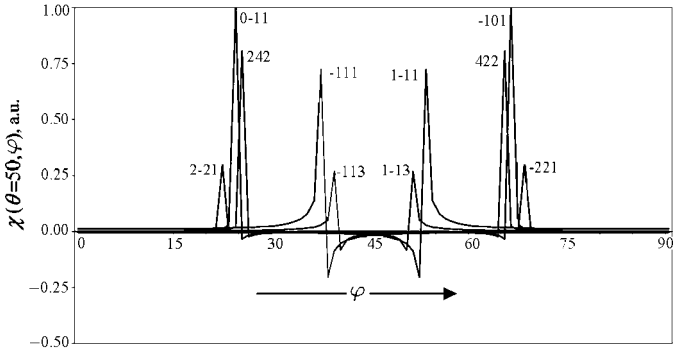

Figure 6
The one-dimensional XFH scan calculated for the fixed value of the elevation angle $\theta = 50^\circ$ is shown as a function of the azimuth angle φ. The diffraction reflections (**h**) mainly contributing to the one-dimensional XFH scan are chosen.

Table 1
Summary of results of the structure-factor restoration using the linear regression algorithm code in the case of the numerically simulated XFH scan for one fluorescing Cu atom incorporated into the small spherical crystalline Cu_3Au cluster.

The 25 crystallographic different structure factors (22 different-valued ones) of the Cu_3Au structure of interest are presented. $F_{true}(\mathbf{h})$ and $F_{rest}(\mathbf{h})$ are the true and restored structure factors, respectively; $\gamma(\mathbf{h}) = |[F_{rest}(\mathbf{h}) - F_{true}(\mathbf{h})]/F_{true}(\mathbf{h})|$ is the relative error; P is the crystallographic plane multiplicity.

h						
H	*K*	*L*	*P*	$F_{true}(\mathbf{h})$	$F_{rest}(\mathbf{h})$	$\gamma(\mathbf{h})$ (%)
0	0	0	1	165.9436	165.9716	0.0169
0	0	1	6	−15.5833	−15.5834	0.0004
1	0	1	12	−14.7474	−14.7474	0.0003
1	1	1	8	131.9148	131.9149	0.0000
0	0	2	6	125.1545	125.1543	0.0003
1	0	2	24	−13.202	−13.202	0.0000
1	1	2	24	−12.8523	−12.8523	0.0004
0	2	2	12	105.7174	105.7173	0.0001
0	0	3	6	−12.0275	−12.0275	0.0005
2	1	2	24	−12.0275	−12.0275	0.0001
1	0	3	24	−11.8034	−11.8031	0.0055
1	1	3	24	95.7682	95.76811	0.0001
2	2	2	8	93.0116	93.0113	0.0003
0	2	3	24	−11.232	−11.2322	0.0011
3	1	2	48	−11.0676	−11.0675	0.0014
0	0	4	6	83.94373	83.98561	0.0501
1	0	4	24	−10.6297	−10.6298	0.0004
2	2	3	24	−10.6297	−10.6297	0.0006
3	0	3	12	−10.4982	−-10.4982	0.0001
1	1	4	24	−10.4982	−10.4982	0.0001
3	1	3	24	78.64503	78.64496	0.0001
2	0	4	24	77.09057	77.09052	0.0004
2	1	4	48	−10.1342	−10.1343	0.0006
3	2	3	24	−10.021	−10.021	0.0004
2	2	4	24	71.69057	71.69043	0.0002

X-ray structure determination. As is pointed out above, an object wave is treated within the scope of the kinematical approach, *i.e.* it is formed as a result of single scattering of a reference wave by neighbouring atoms adjacent to a detecting (fluorescing) atom. Dynamical scattering (primary and secondary extinctions) and absorption of the object wave were not taken into consideration. Besides, the model of the incident unpolarized plane-wave radiation was used to meet the requirements of the linear regression algorithm code. On the other hand, the theoretical calculations may be readily generalized for the case of incident linearly polarized plane-wave radiation; it is a subject of future work. With the above confines of the linear regression algorithm code, we do not claim anything except that the XFH method does work well not using any other information regarding either moduli or phases of the structure factors of interest. How well it will work in practice, particularly taking into account appropriate extinction effects, polarization and coherence properties of the incident X-radiation, remains to be seen and is a topic of future work. Evidently, the corresponding corrections should be introduced into the basic scattering functions to develop and improve the linear regression algorithm code. Another point is that the above theoretical formalism is valid in the case of single fluorescing atoms, which occupy the translation-equivalent crystallographic positions, create the XFH signal and, hence, for such atoms the 'individual' XFH (θ, φ) scans are identical. In this sense, while the gold atoms physically occupy one equivalent position, the copper atoms are located at the three non-equivalent positions in the unit cell of the Cu_3Au structure. Therefore, the XFH (θ, φ) scan with the fluorescing Cu atom is governed by the corresponding average structure factor $\langle F(\mathbf{h})\rangle$, namely: the structure factor $F(\mathbf{h})$ should be substituted by the average one as

$$\begin{aligned}\langle F(\mathbf{h})\rangle &= \tfrac{1}{3}F(\mathbf{h}) \sum_{t=1,\ldots,3} \exp(i\mathbf{h}\cdot\mathbf{r}_t)\\ &= \tfrac{1}{3}F(\mathbf{h})\{\exp[i\pi(H+K)] + \exp[i\pi(K+L)]\\ &\quad + \exp[i\pi(L+H)]\}.\end{aligned}$$

So, strictly speaking, in the case of a fluorescing Cu atom incorporated into the Cu_3Au structure, the average structure-factor set $\{\langle F(\mathbf{h})\rangle\}$ may be the restoration procedure object from the experimental XFH data. It is interesting that, as follows from the above, the phase information for structure factors is unfeasible from the XFH data measured for monoatomic crystals.

Also, testing the linear regression algorithm code, we did not include the noise $\delta(\theta, \varphi)$ that accompanies the XFH (θ, φ) scan in experiment, the value of which is in general given by the XFH counting statistics and might be taken in account with 'structure-factor error' equations (15)–(18). How well they will work for estimating the accuracy of structure factors determined from the XFH data remains to be seen and is of special interest for future work. To be specific, it should be noticed that in practice the noise and other artefacts are removed from the experimental XFH data by filtering (Novikov *et al.*, 1998; Chukhovskii *et al.*, 2002).

It should once more be stated in conclusion that both the feasibility and good skill of the linear regression algorithm direct method tested for the model Cu_3Au structure from a numerically simulated XFH (θ, φ) scan could facilitate further the development of the XFH technique that is of great interest. Noteworthy is the fact that the present treatment shows the great capacity of atom-resolving XFH for structure determinations. By improving the experimental XFH counting statistics and simultaneously solving some theoretical issues mentioned, the atom-resolving XFH method could be favourably applied to structure investigation of low-quality organic single crystals, catalysts or dilute solid solutions. It could become an effective tool for the electron charge-density restoration of crystalline materials and the structure investigation of low-quality organic single crystals, a good topic for future work.

One of authors (FNC) is deeply indebted to Dr B. Adams, Dr R. Eisenhower, Dr D. Novikov, Professor G. Materlik and Professor A. Szöke for fruitful discussions.

References

Adams, B., Nishino, Y. & Materlik, G. (2000). *J. Synchrotron Rad.* **7**, 274–279.

Adams, B., Novikov, D. V., Hiort, T., Kossel, E. & Materlik, G. (1998). *Phys. Rev. B*, **57**, 7526–7534.
Barnard, D. T. & Skillicorn, D. B. (1992). *Effective FORTRAN 77 for Engineers and Scientists*, 2nd ed. Dubuque, IA: Wm. C. Brown Publishers.
Barton, J. J. (1988). *Phys. Rev. Lett.* **61**, 1356–1359.
Barton, J. J. (1991). *Phys. Rev. Lett.* **67**, 3106–3109.
Chukhovskii, F. N., Novikov, D. V., Hiort, T. & Materlik, G. (2002). *Opt. Commun.* **209**, 273–277.
Gabor, D. (1948). *Nature (London)*, **161**, 777–780.
Giacovazzo, C. (1998). *Direct Phasing in Crystallography. Fundamentals and Applications.* IUCr/Oxford University Press.
Gog, T., Bahr, D. & Materlik, G. (1995). *Phys. Rev. B*, **51**, 6761–6764.
Gog, T., Len, P. M., Materlik, G., Bahr, D., Fadley, C. S. & Sanchez-Hanke, C. (1996). *Phys. Rev. Lett.* **76**, 3132–3135.
Gog, T., Menk, R. H., Arfelli, F., Len, P. M., Fadley, C. S. & Materlik, G. (1996). *Synch. Radiat. News*, **9**, 30–35.
Landau, L. D. & Lifshitz, E. M. (1959). *Elektodinamika sploshnych sred*, ch. XV. Moscow: GIFML. (In Russian.)
Landree, E., Collazo-Davila, C. & Marks, L. D. (1997). *Acta Cryst.* B**53**, 916–922.
Novikov, D. V., Adams, B., Hiort, T., Kossel, E., Materlik, G., Menk, R. & Walenta, A. (1998). *J. Synchrotron Rad.* **5**, 315–319.
Szöke, A. (1986). *Short Wavelength Coherent Radiation: Generation and Applications*, edited by D. T. Attwood & J. Bokor. *AIP Conf. Proc.* No. 147, pp. 361–476. New York: American Institute of Physics.
Tegze, M. & Faigel, G. (1991). *Europhys. Lett.* **16**, 41–44.
Waasmaier, D. & Kirfel, A. (1995). *Acta Cryst.* A**51**, 416–431.